ELSEVIER

Astroparticle Physics 8 (1998) 179–191

Astroparticle Physics

A search for TeV gamma-ray bursts on a 1-second time-scale

V. Connaughton [a,b,*], C.W. Akerlof [c], S. Biller [d], P. Boyle [b], J. Buckley [a], D.A. Carter-Lewis [e], M. Catanese [e], M.F. Cawley [f], D.J. Fegan [b], J. Finley [g], J. Gaidos [g], A.M. Hillas [d], R.C. Lamb [e], R. Lessard [b], J. McEnery [b], G. Mohanty [e], N.A. Porter [b], J. Quinn [b], H.J. Rose [d], M.S. Schubnell [c], G. Sembroski [g], R. Srinivasan [g], T.C. Weekes [a], C. Wilson [g], J. Zweerink [e]

[a] *Whipple Observatory, Harvard-Smithsonian, CA, USA*
[b] *University College, Dublin, Ireland*
[c] *University of Michigan, USA*
[d] *University of Leeds, UK*
[e] *Iowa State University, USA*
[f] *St.Patrick's College, Maynooth, Ireland*
[g] *Purdue University, USA*

Received 20 May 1996; revised 10 October 1997; accepted 10 October 1997

Abstract

Although atmospheric Cherenkov telescopes have restricted fields of view, their fluence sensitivity warrants a search for gamma-ray burst phenomena. A search for 400 GeV gamma-ray bursts on a 1 s time-scale using archival data taken between 1988 and 1992 with the Whipple Collaboration 10 m reflector is presented. No evidence of such bursts is found. Bursts of TeV gamma rays have been predicted from exotic astrophysical objects such as Primordial Black Holes and Cosmic Strings. An upper limit to the number density of exploding PBH of $3.0 \pm 1.0 \times 10^6$ pc^{-3} yr^{-1} is calculated. © 1998 Elsevier Science B.V.

PACS: 95.75.-z; 95.85.Pw; 98.70.Rz; 98.62.Nx
Keywords: TeV astronomy; Gamma-ray bursts; Primordial black holes

1. Introduction

The detection of gamma-ray bursts with peak luminosity at MeV energies has been one of the most exciting discoveries in high-energy astrophysics [9]. Although still unexplained after 30 years of intense research, the phenomenon has inspired searches for counterparts at a variety of wavelengths [14]. It has also opened the possibility that there might be similar phenomena that have peak luminosity at other wavelengths; here we consider a TeV search for such phenomena on time-scales of one second using the Imaging Atmospheric Cherenkov Technique.

The Whipple Observatory Gamma Ray Collaboration has been involved in searches for gamma-ray bursts since 1978; initially, multi-element first generation systems over long baselines were used [17]. The development of the Imaging Atmospheric Cherenkov

* Corresponding author. ES84, Marshall SpaceFlight Center, AL 35812, USA; E-mail: vc@msfc.nasa.gov.

PII S0927-6505(97)00055-8

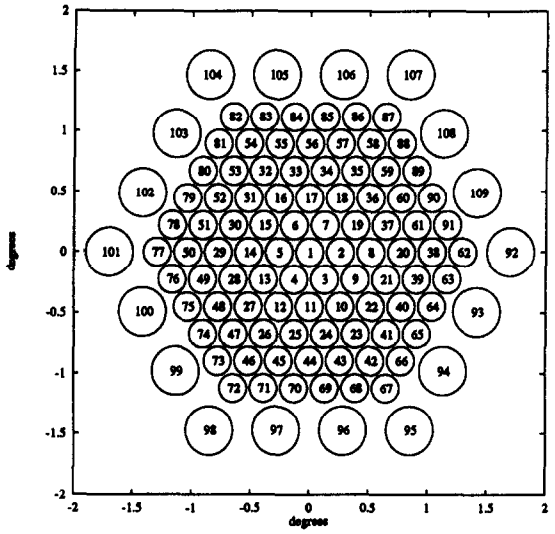

Fig. 1. Arrangement of photomultiplier tubes in focus box of 10 m reflector.

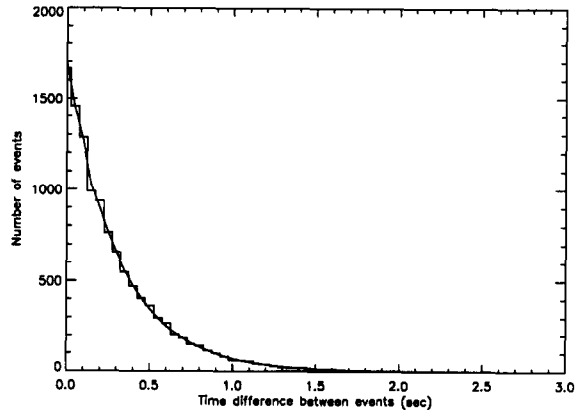

Fig. 2. Arrival time difference distribution of successive events in a 60 minute data file (histogram). The solid curve shows the expected Poisson distribution for this average event rate and total number of events.

Technique has significantly improved the sensitivity for the detection of point sources [25]. The Whipple 10 m imaging camera has successfully detected TeV emission from several point sources - the Crab Nebula [24], Markarian 421 [19], and Markarian 501 [20]. It has been the most sensitive instrument of its kind for source-centered observations but its off-axis sensitivity has not so far been fully characterized [1].

Here the response of the Whipple 10 m reflector to non-source-centered gamma rays is assessed using shower simulations, and a method is developed to search for gamma-ray bursts of one second duration. We report on a search through 4 years of the Whipple database.

There are a number of exotic suggestions that justify a search for gamma-ray bursts in this parameter space. These include emission from the decay of primordial black holes (PBHs) [13] and cosmic strings [22]. The cosmological and physical importance of PBHs is well established [12]. As the PBH evaporates, its temperature increases in proportion to the mass loss. Most models predict a final explosion of energy when all possible evaporation channels are available, but the number of degrees of freedom of emission is a highly controversial issue, and ranges from the conservative standard elementary particle model, where it reaches a maximum once the three generations of fermions are free to be produced, to the runaway Hagedorn model where the number of emission modes increases exponentially beyond this [12]. For the conservative model, an optimum time-scale of 1 s is found for observing the explosion of a PBH using the Whipple 10 m telescope. During this final second 9.1×10^{28} photons are emitted above 0.4 TeV.

The fluence sensitivity of the detector over this time-scale is of order 10^{-9} erg cm^{-2} which is comparable to or better than that achieved in most bands of the gamma-ray spectrum. The sensitivity of the technique is compared to that achieved in searches by other gamma-ray experiments, operating at energy thresholds higher than the Whipple instrument.

2. The Whipple 10 m telescope

Situated at an altitude of 2.3 km on Mt.Hopkins in Arizona, the telescope operated by the Whipple Collaboration has been used as an imaging device since 1982; the camera has been improved from a 37 to a 109 element imaging system during that time. The telescope consists of a 10-metre dish (with 248 front-coated mirrors) on an alt-azimuth mount and a camera containing 109 photomultipliers (PMTs). The inner 91 PMTs are 1.1 cm diameter tubes (Hamamatsu R1398) and are connected via amplifiers to trigger discriminators. An outer ring of 18 tubes is independent of the trigger logic and contributes only to the

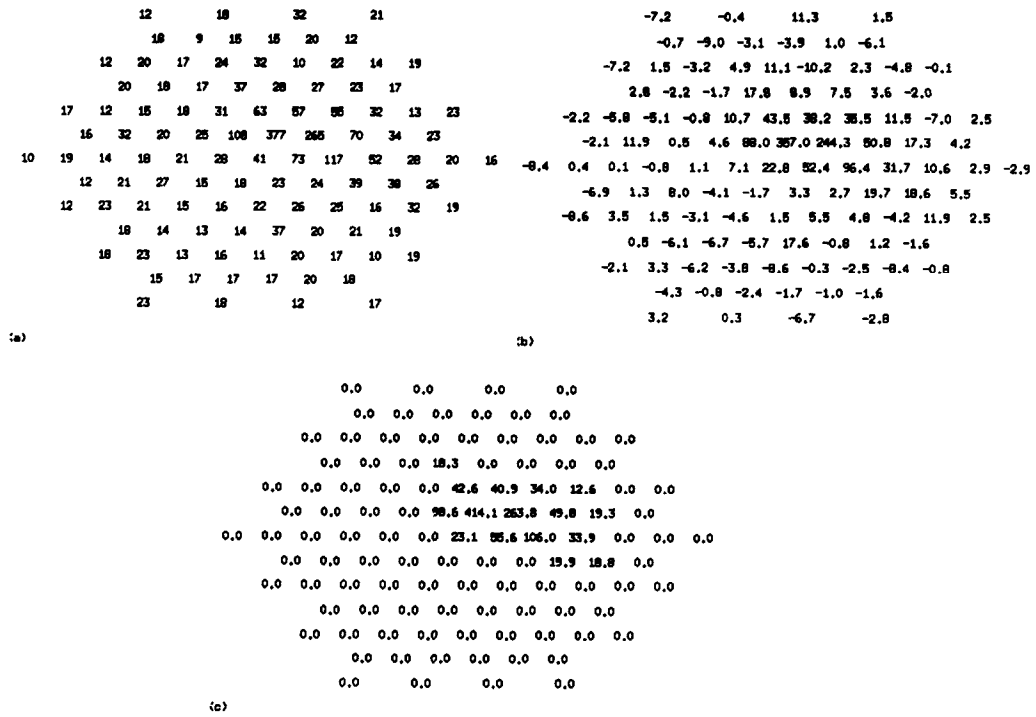

Fig. 3. 10 m image (a) before and (b) after flat-fielding, and (c) after cleaning.

imaging of the event. Until 1993, these outer tubes were 5 cm tubes giving a total field-of-view of 3.75°. They have been replaced by the smaller tubes so that the camera field-of-view is now 3°. The arrangement of PMTs in the focus box prior to 1993 is shown in Fig. 1 and a detailed description of the instrument can be found in [5].

The camera is triggered if the signal in two or more PMTs exceeds a preset threshold in a 10 nsec time interval. When the system is triggered, i.e. an event is registered, the light level in each PMT is recorded over a 25 nsec gate width. The trigger rate during the epoch of the observations reported here was typically 8 events per second. The time is derived from a GPS clock and is recorded with each event with an accuracy of 0.1 msec. The deadtime is 1.5 msec and the distribution of time differences of successive events from a 60 minute data file taken at a telescope elevation of 80° is shown in Fig. 2 (histogram). It is overlaid on the expected Poisson distribution for the same mean event rate (solid curve).

The digitized images of the Cherenkov light are analyzed off-line. A typical image recorded by the present

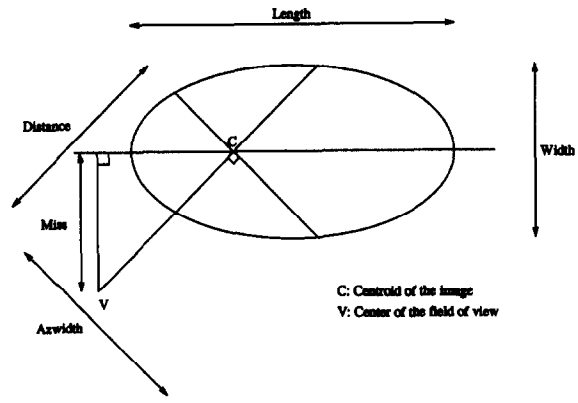

Fig. 4. Representation of image parameters.

camera is shown at various stages of processing in Fig. 3. Moment-fitting routines are used to define each image by an ellipse whose parameters define the event (shown in Fig. 4). The event is accepted as a potential gamma-ray event or rejected as a hadron-initiated event depending on the values of these parameters. The axis of the image is defined by minimizing the signal-weighted sum of the squares of the perpendicular angular distances of the pixels. The r.m.s. spread

of light perpendicular to and along this axis defines the semi-minor and semi-major axes of the ellipse and these are known as the *width* and *length* of the image. Image compactness is defined by *concentration*, which is the fraction of the sum over all nonzero pixels of the cleaned image in digital counts (known as *size*) contained in the two or three brightest pixels. The other parameters shown in Fig. 4 relate to the orientation of the image axis relative to the source position in the field-of-view.

If the position of the source is known (usually at the centre of the field of view), then the orientation of the image relative to that direction is important for source detection. A combination of shape and orientation parameters has been used by the Whipple Collaboration to reject 99.7% of recorded background while keeping 50% of gamma rays; the set of selection parameters that are most useful for observations of a point-source in the centre of the field of view are called Supercuts and are defined elsewhere [21]. A comparison of the *width* and *length* domains for photons (simulated) and real background (data taken with the telescope pointed at the zenith) can be seen in Fig. 5.

The success of Supercuts and the Imaging Atmospheric Cherenkov Technique in the detection of point sources owes much to Monte Carlo simulations of photon and background hadron-initiated cascades. Owing to the impossibility of testing the atmospheric Cherenkov detector at an accelerator, analytical models and simulation of phenomena are used to optimize instrumental design and in the development of analysis techniques. Data taken during observations of the Crab Nebula, which plays the role of a TeV gamma-ray standard candle, are used to perfect new techniques.

3. Off-axis sensitivity of 10 m reflector

The characteristics of the 10 m reflector in point-source mode of operation are well understood and defined [5]. What is less well characterized is the sensitivity of the instrument when an area of the sky is probed for a source without knowing its exact position, i.e., where each point in the field-of-view is a potential source. It has been demonstrated experimentally that the system is sensitive to a point source of gamma rays up to 1° off-axis [1,10]. In the work reported here, the response over the full field-of-view of the 10 m reflector is investigated, using simulations, in order to use the instrument as a relatively wide field burst detector.

3.1. The off-axis triggering and imaging of gamma rays

The geometrical field-of-view of the 10 m camera between 1988 and 1992 was 3.75°, but the imaging technique allows reconstruction of images whose origins lie outside this area. Conversely, some of the images of showers from sources on the edge of the camera face may fall outside the field-of-view so that the camera has reduced collection area for such sources.

In order to assess the sensitivity of the instrument for sources lying at various distances from the centre of the camera, a database of nearly 8000 simulated gamma-ray-induced showers of energies ranging from 0.2 TeV to 0.8 TeV was compiled using a simulation program based on the KASCADE code of Kertzmann and Sembroski [15]. The Whipple collaboration has used several different simulation codes in the various research institutions (e.g. MOCCA at the University of Leeds) and comparison of the simulations shows that they are in agreement with each other to within 10% in the Cherenkov light yields and image parameter distributions that they produce.

The response of the instrument to the simulated gamma-ray showers is gauged by mapping each Cherenkov photon in a shower from the mirrors onto the imaging camera and building up an event for each shower.

Displacing the focus box from its position at the focus of the reflector and constructing events as they appear to this displaced camera is equivalent to simulating the response of the camera to sources at an offset from the centre equal to the displacement of the camera but in the opposite direction. The response of the camera to gamma-ray showers from sources with 0° to 2.5° offsets from the centre was investigated by successively displacing the camera at 0.25° intervals along an arbitrary line, 17° from an axis through the centre of a row of PMTs. A different source displacement angle may be chosen without affecting the results. The treatment of simulated images is identical to that subsequently applied to real data. The parameterization and cutting procedures execute rapidly relative to the shower and instrument simulations, and it

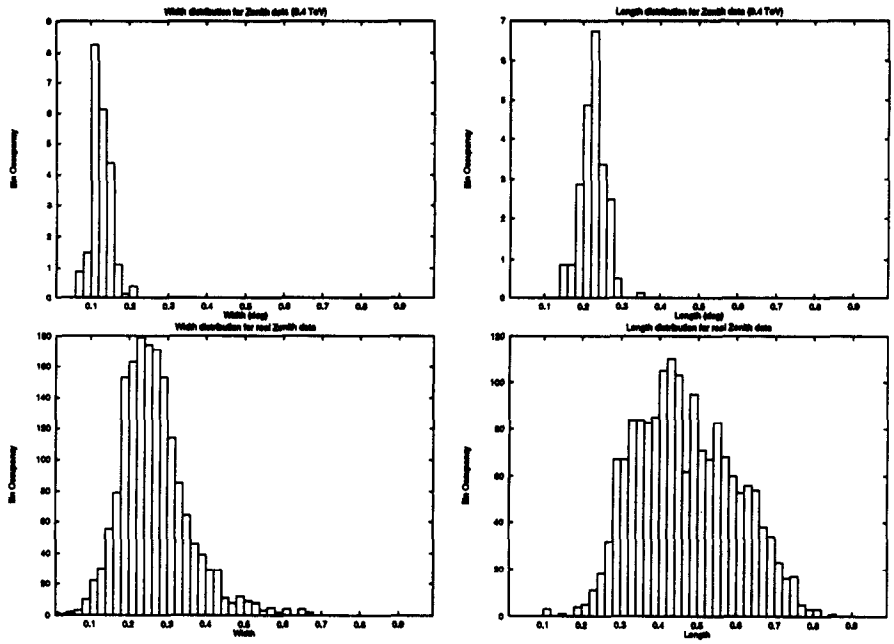

Fig. 5. Width (left) and length (right) distributions for simulated 0.4 TeV photon from the zenith (top) and real zenith (bottom) showers.

was possible to experiment with a variety of parameters and analysis methods before deciding on a suitable gamma-ray burst search method.

As the source position moves further away from the centre of the camera, less Cherenkov light falls on the detector at a given impact parameter. The software trigger is a requirement that two of the inner 91 tubes register at least 40 photo-electrons and the percentage of events triggering the system at each impact parameter is shown in Fig. 6 for source offsets of (a) 0°, (b) 0.75°, and (c) 1.5°.

By weighting the fraction according to the impact parameter value (the collection area is bigger at larger impact radii), a value for the trigger efficiency over the field of view, equivalent to the effective area of the detector for each source offset, is calculated,

$$\text{Trigger efficiency} = \frac{\sum_i 2\pi r_i \phi_i \, \delta r}{7 \times 10^4}, \qquad (1)$$

where r_i $(= i)$ is the radius of the annulus at impact parameter i, thickness $\delta r = 2$ metres, and ϕ_i is the fraction of the 20 showers at radius r_i which would trigger the telescope. The summing integer i is incremented from 12 to 200 in steps of 2. At impact parameters below 10 metres, the showers tend to saturate the central tube, and the Cherenkov light pool falls off rapidly beyond 150 metres, so that we define an ideal detector as one which is triggered by all showers with impact parameters between 10 and 150 metres, and which fails to register any events falling outside that area. The trigger efficiency is divided by 7×10^4 m^2 to give the efficiency relative to this arbitrary ideal detector. An efficiency of greater than 1 is, therefore, possible since showers lying beyond 150 metres may trigger the system. This procedure was implemented for all 4 shower energies, and the results are shown in Fig. 7. Above threshold (> 0.4 TeV) the instrument would register over half of the gamma-ray showers from sources out to 1° away from the centre, but it is obviously more efficient at detecting those nearer the centre than at large offsets.

Image parameters have traditionally been used, in some combination of shape and orientation cuts, to discriminate against the hadronic background. In this search, however, only the shape parameters are relevant since there is no preferred direction due to the unknown position of the source in the field-of-view. The most successful shape selection was found to involve cuts in *length* and *width*, using the values derived for Supercuts,

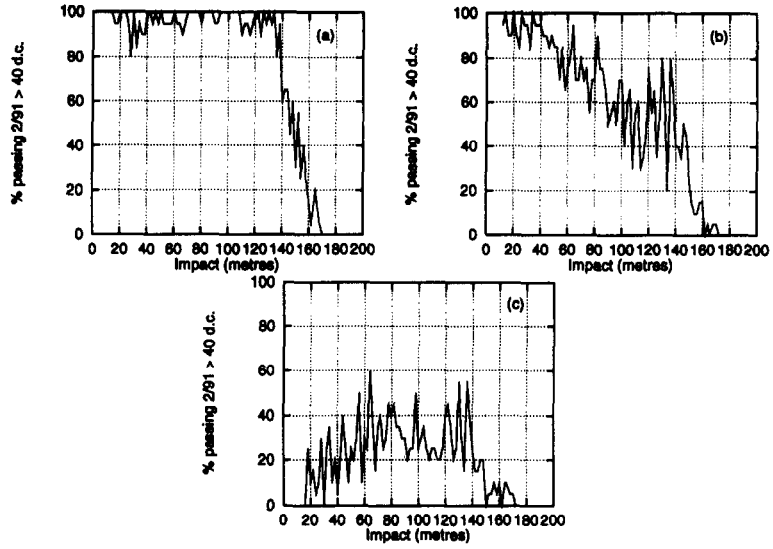

Fig. 6. Percentage of events which trigger the 10 m reflector as a function of impact parameter for source offsets (a) 0°, (b) 0.75°, (c) 1.5° for 0.4 TeV showers.

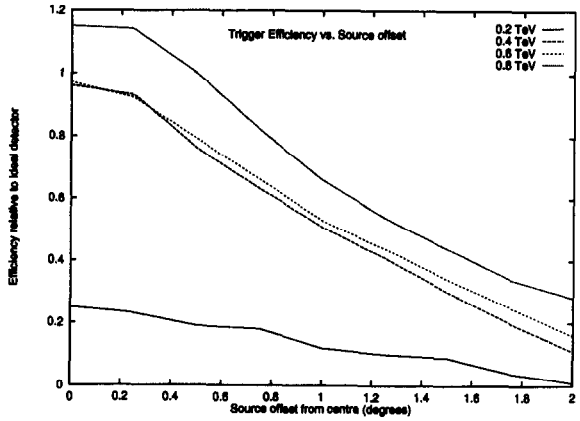

Fig. 7. Trigger efficiency of the 10 m reflector as a function of source offset and energy. An efficiency of 1 is that of an ideal detector which has a 100% trigger rate for showers of impact parameters between 10 and 150 metres, and no triggers outside this range. This is equivalent to a collection area of 7×10^4 m^2.

$0.073° < width < 0.15°$,

$0.16° < length < 0.30°$.

Fig. 8 shows the percentage of 0.4 TeV events at offsets (a) 0°, (b) 0.75° and (c) 1.5° which trigger the camera and satisfy these image shape requirements. Combining the percentages for each impact parameter produces the results which are shown in Fig. 9. Above the detector energy threshold, the collection area for gamma rays is fairly flat, and showers from sources which are up to half a degree off-axis are still selected over 50% of the time. There are two competing effects which explain the shape of the curves: at high energies, showers with large impact parameters produce enough Cherenkov light to trigger the telescope more often than distant low-energy showers, but the Supercuts selection is biased towards small showers, so that the higher energy showers are less likely than the low-energy events to survive the *width* and *length* cuts regardless of impact parameter. At large source offsets the fraction of events selected decreases with shower energy even though the high-energy events appear to trigger the camera more often than at lower energies. If the showers triggering the system at these large offsets are examined, it can be seen that they are the longest images in the high-energy databases.

Observations of the Crab Nebula at angular offsets from the centre of the field-of-view of the 10 m telescope were used to confirm the efficiency curves derived from these simulations. The Crab Nebula is a steady source of TeV gamma rays, and by comparing the rate of gamma rays measured after applying the Supercuts selection technique to data from September 1996 at offsets ranging from 0° to 1.5°, one obtains the efficiency for gamma ray collection displayed in Fig. 10. The errors in Fig. 10 reflect the variation in

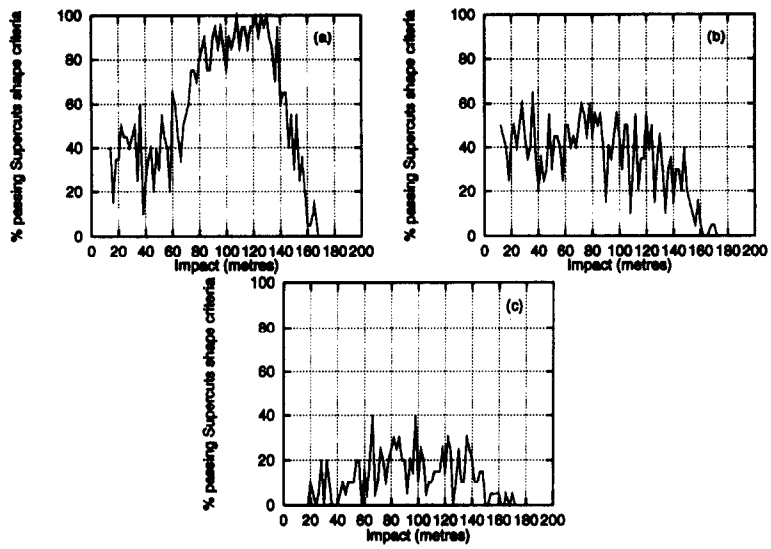

Fig. 8. Percentage of events which survive Supercuts shape cuts as a function of impact parameter for source offsets (a) 0°, (b) 0.75°, (c) 1.5° for 0.4 TeV showers.

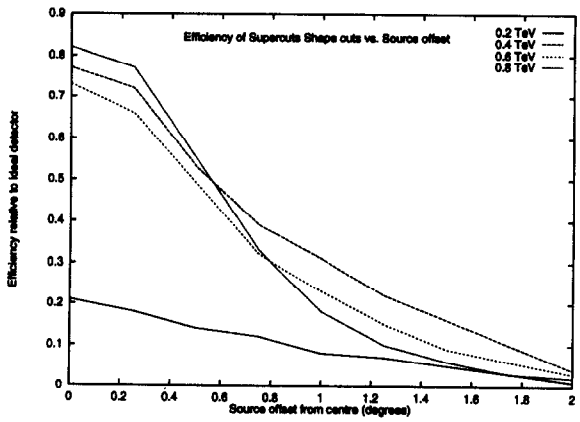

Fig. 9. Ability of 10 m reflector to detect gamma rays as a function of source offset and energy. *Width* and *Length* cuts are made on all events that trigger the system. An efficiency of 1 is that of an ideal detector which has a 100% trigger and image selection rate for showers with impact parameters between 10 and 150 metres and none outside. This is equivalent to a collection area of 7×10^4 m^2.

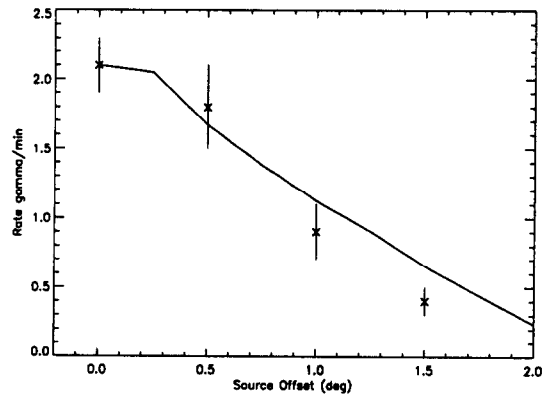

Fig. 10. Efficiency curve from simulations (solid line) compared to the gamma-ray rate measured from Crab Nebula (x) as a function of source offset.

event rates for the offset observations, and are large owing to the small exposure time: only 1 hour of source observations was made at a source offset of 0.5° from the centre of the field-of-view, 1.5 hours at 1.0°, and 2 hours at 1.5° offset. Because the field-of-view of the telescope was smaller when these offset observations were made compared to that simulated in this study, a perfect correlation is not expected, and one anticipates that the efficiency at larger source offsets be slightly lower relative to source-centered observations than in the simulations.

3.2. Orientation of gamma-ray images

The orientation of the ellipse fitted to each image is represented by its major axis, and the most likely point-of-origin of the shower progenitor on the field-of-view lies on this axis at a distance d in degrees

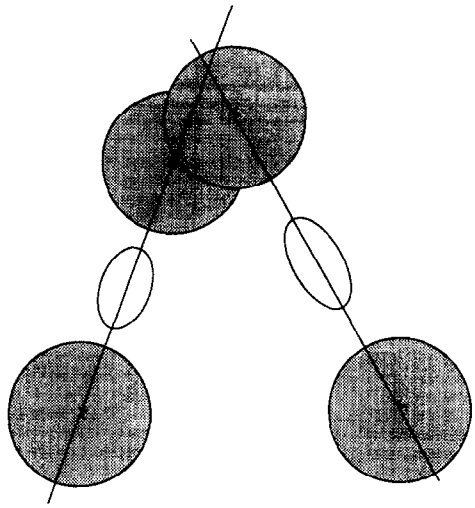

Fig. 11. Illustration of the most likely points-of-origin (x) along the major axes of two events (ellipses). The shaded circles indicate the uncertainty associated with these positions.

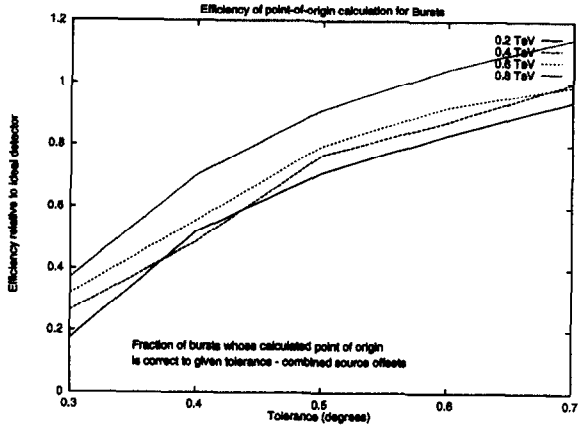

Fig. 12. Efficiency of point-of-origin determination from $d = 2 - 2 \times width/length$ along the major axis. The tolerance on the x-axis is the value by which this calculated point-of-origin is allowed to vary from the actual source position.

related to the ellipticity of the image,

$$d = 2 - 2(width/length)\,. \tag{2}$$

This algorithm was developed based on simulations of gamma-ray showers from sources at the centre of the field-of-view, and was found to be accurate to about 0.3° either side of this point [1] for source-centered observations. The relation between the image, its centre, and the most likely point-of-origin are shown in Fig. 11.

Because the ellipses derived from the moment-fitting routines are symmetrical, the point-of-origin may lie either side of the centre of the image. The following equations are used:

$$\sqrt{(y_{or} - y_{cen})^2 + (x_{or} - x_{cen})^2} = 2 - 2 \times width/length\,,$$

$$y_{or} = m \times x_{or} + c\,,$$

to find the most likely points-of-origin x_{or}, y_{or} on both sides of the centre of light x_{cen}, y_{cen} along the major axis $y = m \times x + c$. The distance

$$\sqrt{(y_0 - y_{or})^2 + (x_0 - x_{or})^2}\,, \tag{3}$$

where x_0, y_0 are the true positions of the simulated source, is a measure of how well Eq. (2) finds the point-of-origin of a shower. The tolerance is defined as the maximum allowed value of this distance, in degrees. A range of tolerance levels from 0.1° to 0.7° was explored to determine the off-axis efficiency of the point-of-origin determination, and the results are displayed in Fig. 12. The total efficiency Φ for each energy was obtained by combining source positions and weighting each efficiency (ϕ_r) according to source offset (r). The efficiency values featured are relative to an ideal detector with $\phi_r = 1$ at each source offset where the gamma-ray images are selected and their origin is correctly determined so that $\Phi = \sum \phi_r r / \sum r$, with r varying from 0.25° to 2.5°. The efficiency curve is fairly constant as the source is moved away from the centre and appears independent of impact parameter and photon energy.

Real background data were subjected to the same analysis so that the effect of varying the point-of-origin tolerance value on background acceptance could be assessed. It was found that in looking for bursts of 3 or more events over a 1-second time-scale, the highest signal to noise ratio could be obtained with a tolerance level of 0.425°. This selection criterion enables $66 \pm 5\%$ of shape-selected simulated events (over the impact parameter range 12 to 200 metres and source offset 0° to 2.5°) to be correctly located. The shaded areas in Fig. 11 show the regions from which the imaged events could have originated with this tolerance value.

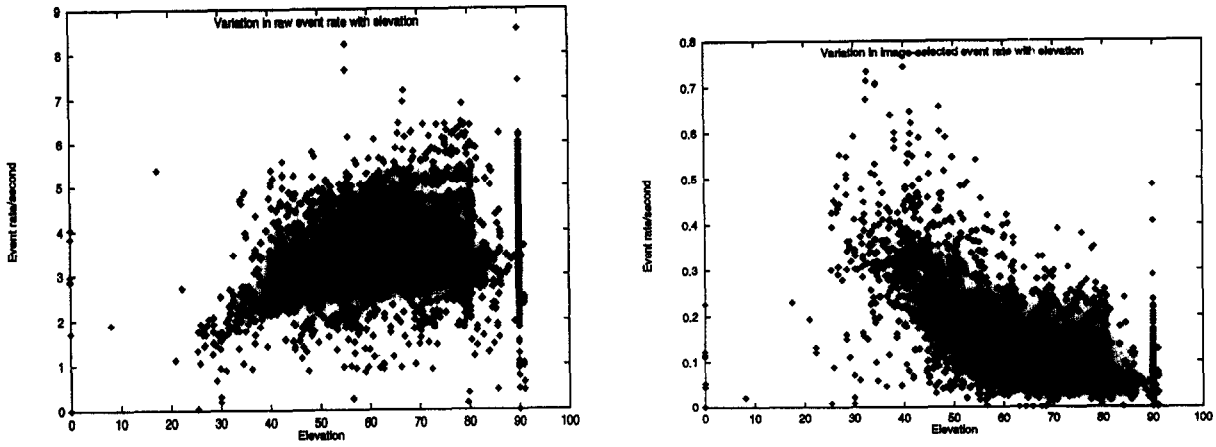

Fig. 13. Variation of event rate with elevation raw event rate (left) and event rate after selection via image *width* and *length* cuts (right).

It is then possible to apply this calculated off-axis response of the detector to the search for counterparts to the delayed component of BATSE bursts (reported elsewhere [7]) and to the serendipitious detection of gamma-ray bursts during the normal operation of the gamma-ray telescope (described below).

4. Searches for 1 s TeV gamma-ray bursts

The archival data of the Whipple Observatory taken with the 10 m reflector with an energy threshold above 0.4 TeV between September 1988 and September 1992 were used for this search. In general these observations were in the form of files of (approximately) 28 minute duration containing information on each event (the arrival time, the outputs of the 109 ADCs from the 109 pixels, and other housekeeping data). Examination of the observing logs allowed the identification and rejection of 1% of the data including (i) observations made when there were instrumentation problems, (ii) data taken with discriminator thresholds or high-voltage values significantly different from those used in normal operation, and (iii) observations made while testing new or experimental configurations (for example, experiments with filters). A further 1% of the files were rejected because of obvious anomalies, such as a large number of bright stars in the field-of-view, or because they were taken at a telescope elevation less than 35° above the horizon. Following rejection of unsuitable data, 2217 hours of observations comprised the database. The database was divided according to the event rate of candidate gamma rays. Variation in event rates was caused by differences in zenith angle, mirror reflectivity and discriminator settings. The elevation of the source under observation is known to affect the energy threshold of the detector, and also influences the appearance of both gamma and hadronic images. A larger depth of atmosphere must be penetrated by the extensive air shower particles if they are to produce light lower in the atmosphere, so that a telescope pointed close to the zenith is sensitive to lower energy showers than if it is operated nearer the horizon. Consequently, the raw event rates decrease with increasing zenith angle – this relationship is shown in Fig. 13 (left). Despite this overall fall in event rates at low elevations, the Cherenkov image on the camera face is narrower on the horizon than at the zenith, and this effect results in more hadronic events being selected as gamma rays on the basis of the *width* parameter. Fig. 13 (right) shows the variation of image-selected event rate with telescope elevation.

Nearly 80% of observations were made with the telescope elevation above 55°, where data rates and image characteristics are fairly homogeneous. These observations form the bulk of the 1759 hours of data which had an average rate of < 0.2 candidate gamma-ray events per second, and comprise the largest of the three subsets of the Whipple database. The rest of the data was divided according to the average event rate; rate = 0.2 to 0.4 per second (394 hours) and rate $>$ 0.4 events per second (64 hours). Standard routines were used to flat-field the data, tubes with bright stars

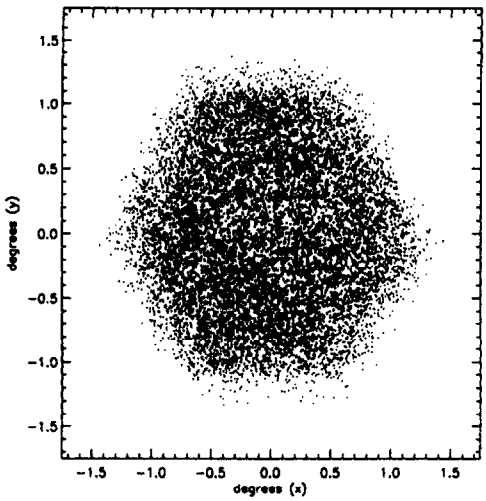

Fig. 14. Event centroid distribution of events in a 60 minute data file.

in their field-of-view were turned off in hardware or software, and the image parameters were calculated as described in [21]. The events were then characterized by these image parameters (and their arrival times). The evenness of the camera response across the field-of-view is illustrated in Fig. 14, showing the distribution of event centroids in camera coordinates (degrees from centre) for a 60 minute observation.

4.1. The burst search

Initially the events were culled to include only those events whose images satisfied the gamma-ray event criteria. Events which survived the *width* and *length* cuts described above were included in a reduced data set which was submitted to a search for bursts of 3 or more events in a 1 s time interval.

The arrival time of the first event was taken as the possible start of a 1 s burst and was compared to the time of the second event. If the time difference was under 1 s, the next event was examined. If not, the start of the time window was moved to the arrival time of the second event. The window was moved through the file until all events in a file have been processed, and the total number of bursts with from 3 to 10 shape-selected events in the file is obtained. No candidate bursts were found with more than 4 events. The number of 3- and 4-fold burst events are shown in Table 1 in the column headed "obs". A background (control) file was generated from each real data file by scrambling the events in each parameterized file, while maintaining the original time sequence. When the background file was subjected to the burst-search program, the image-selected events were the same as those picked from the real data file, but in a random order and attached to the original arrival times of other events. The number of 3- and 4-fold bursts thus found is shown in Table 1 headed "exp". The difference between the observed and the expectation is expressed in terms of the standard deviation, σ defined as $(\text{obs} + \text{exp})^{1/2}$. In no case is the difference statistically significant.

To this point no use has been made of the fact that the events in the putative 3- and 4-fold bursts must come from the same point in the sky. Hence all the bursts were subjected to the common origin selection described above. Less than 2% of the putative bursts passed this selection. These are listed as before in Table 2; the expectation is derived by applying the common origin selection to the scrambled events.

Again, no excess of 3- or 4-fold bursts of candidate gamma-ray events on a 1-second time-scale is found in the 2217 hours of the Whipple database. Two candidate four-fold events are shown in Fig. 15. If a TeV component to a background of bursters exhibiting activity on a 1 s time-scale exists, then the number of these bursts is low and below the sensitivity of the instrument in its current form.

5. Upper limit to density of exploding PBH

Based on the null results obtained in this search, an upper limit to the local density of exploding PBHs can be calculated using the flux of TeV photons predicted by the standard model and presented in [12].

Previous results of searches for exploding PBH by the Whipple Collaboration used extrapolated values of collection area and solid angle [18,16,23,6]. The work presented here involves a search over a larger archival database (2217 hours) for bursts on a longer time-scale (1 s) with a lower energy threshold (0.4 TeV); hence the sensitivity should be greater. In addition the sensitivity is calculated more rigorously than in previous experiments. In the earlier Whipple experiments the sampling distance was calculated from the trigger efficiency rather than gamma-ray collection area. Our new Monte Carlo simulations indicate that in calculat-

Table 1
Frequency of gamma-ray burst candidates in Whipple database vs expected burst frequency (no common origin sought)

Event rate/sec (cut)	Hours of data	3-event burst			4-event burst		
		exp	obs	σ	exp	obs	σ
0.0–0.2	1759	4747	4762	+0.15	234	245	+0.50
0.2–0.4	394	13463	13679	+1.31	1308	1286	−0.43
> 0.4	64	10597	10539	−0.40	1800	1724	−1.28
Total	2217	28807	28980	+0.72	3342	3255	−1.07

Table 2
Frequency of gamma-ray burst candidates in Whipple database vs expected burst frequency (with common origin)

Event rate/sec (cut)	Hours of data	3-event burst			4-event burst		
		exp	obs	σ	exp	obs	σ
0.0–0.2	1759	62	73	+0.95	0	2	1.41
0.2–0.4	394	230	232	+0.09	8	5	−0.83
> 0.4	64	236	257	+0.95	12	5	−1.70
Total	2217	528	562	+1.03	20	12	−1.41

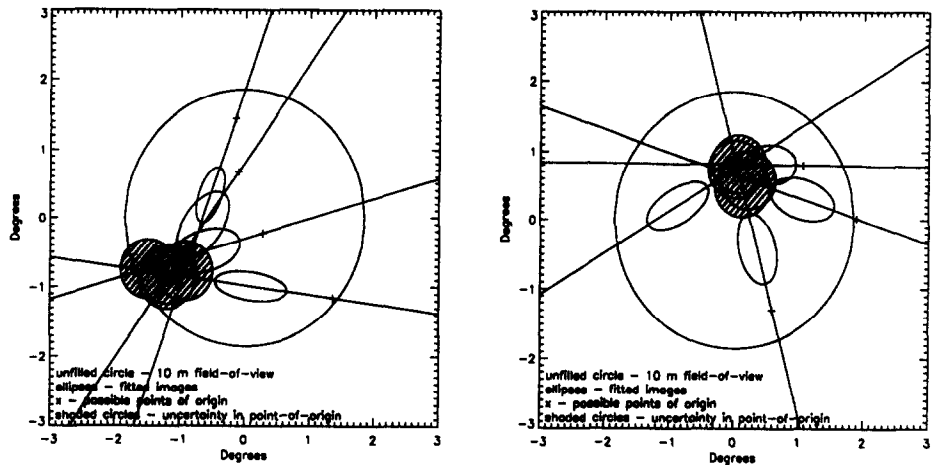

Fig. 15. Two bursts of four events from real data in 1 second with a possible common point-of-origin.

ing limits from data taken after 1988 (when the imaging system was introduced), the sampling distance was overestimated. In addition, a constant gamma-ray sensitivity over the field-of-view was assumed and the sensitive volume integrated the estimated sampling distance over the solid angle of the camera. A more realistic sensitive volume based on Monte Carlo simulations is used in this search. Table 3 shows the sampling distances and sensitive volumes for a 3-photon burst in the 10 m reflector for source offsets out to 2° given the gamma-ray flux calculated in [12]. The second column shows the collection area for a source at a particular point in the camera and column 3 shows the maximum distance at which a PBH can be detected. The volume probed, V_i, is calculated by integrating over the solid angle, Ω_i, covered by the annulus (or circle for a source at the centre) described by the source offset: $V_i = \frac{1}{3} r_i^3 (\Omega_i - \Omega_{i-1})$. This volume

Table 3
Sensitivity of 10 m reflector for 0.4 TeV γ after applying *width* and *length* cuts at source offsets out to 2°

Source offset from center (°)	Collection area (10^4 m^2)	Sampling distance (pc)	Sensitive volume ($\times 10^{-6}$ pc^3)
0.00	5.39 ± 0.89	0.38 ± 0.15	1.09 ± 0.07
0.25	5.07 ± 0.89	0.37 ± 0.15	3.03 ± 0.20
0.50	3.69 ± 0.95	0.32 ± 0.16	3.27 ± 0.41
0.75	2.73 ± 0.94	0.27 ± 0.16	2.75 ± 0.57
1.00	2.14 ± 0.82	0.24 ± 0.15	2.48 ± 0.61
1.25	1.52 ± 0.78	0.20 ± 0.14	1.75 ± 0.60
1.50	1.15 ± 0.62	0.18 ± 0.13	1.51 ± 0.57
1.75	0.70 ± 0.48	0.14 ± 0.11	0.82 ± 0.40
2.00	0.31 ± 0.37	0.09 ± 0.10	0.25 ± 0.34
Total sensitive volume			16.95 ± 3.77

Table 4
Upper limits to exploding PBH frequency from archival search

Hours of data	3-event burst		4-event burst	
	volume $\times 10^{-5}$ pc^3	limit $\times 10^6$ pc^{-3} yr^{-1}	volume $\times 10^{-5}$ pc^3	limit $\times 10^6$ pc^{-3} yr^{-1}
1759	1.67 ± 0.38	14.13 ± 3.3	1.07 ± 0.26	3.0 ± 1.0
394		96.2 ± 23.0		20.4 ± 5.3
64		745 ± 170		117 ± 30

is nearly 8 times smaller than the volume estimate in Nolan et al. [16] although the hardware system is identical and the analysis and burst search methods used in this work are more sensitive.

The corresponding distances and volumes accessible to the reflector can be calculated for the detection of bursts of 4 photons in 1 s. The excess (or deficit) of bursts obtained over expectation in the sensitive volume in each of the three data groups in the archive is used to find the 99.9% maximum likelihood upper limit to the frequency of exploding PBH per year per cubic parsec (Table 4). More sensitive upper limits are obtained from air shower experiments which operate at higher energies and have longer exposure times; these are shown in Table 5.

Models other than those derived from standard elementary particle theory have also been invoked to describe the final stages of evaporation of a PBH. Those propose a faster process with more degrees of freedom than the standard model – the Hagedorn model, in which the number of degrees of freedom increases exponentially with the number of emitted particles, predicts the most catastrophic explosion, of 6.0×10^{34} erg, lasting only 10^{-7} seconds, and comprised mainly of 250 MeV photons. A larger volume is accessible to searches for this type of event than for PBH exploding according to the standard model. Upper limits to Hagedorn-type PBH explosions are, therefore, more restrictive, and are given in [17,8].

Table 5
Standard elementary particle upper limits to PBH density

Experiment	Energy (TeV)	Ref.	Limit (pc^{-3} yr^{-1})
CYGNUS	50	[2]	6.1×10^5
AIROBICC	20	[11]	8.9×10^5
Tibet	10	[3]	4.6×10^5

6. Conclusions

A method is described of using an atmospheric Cherenkov telescope to search for gamma-ray bursts on short time-scales. The application of this method to the search for counterparts to classical gamma-ray bursts detected by the BATSE experiment is described

elsewhere [7]. Here it is applied to a search through a four year database accumulated by the Whipple telescope in its routine discrete source observing program. The minimum detectable fluence (6×10^{-9} erg cm^{-2} in one second) is comparable with that of BATSE at much lower energies and compares favorably with all other gamma-ray experiments currently in operation.

Null results are obtained and an upper limit to the PBH density is derived, where the PBH is exploding via the standard model. This limit of $3.0 \pm 1.0 \times 10^6$ pc^{-3} yr^{-1} is better than that obtained from previous searches using the Whipple 10 m reflector. It is not, however, as stringent as the PBH limits obtained with wide field air shower experiments. The low duty cycle and small field-of-view of atmospheric Cherenkov telescopes makes them less efficient than air shower experiments like the MILAGRO water-Cherenkov telescope [4] which have a large field-of-view and longer exposures. Telescopes with rapid slew speeds are, nevertheless, well suited for the detection of very high-energy counterparts to BATSE-type bursts [7].

Acknowledgements

We acknowledge the technical assistance of Teresa Lappin and Kevin Harris. This research is supported by grants from the US Department of Energy and by NASA, by PPARC in the UK, and by Forbairt in Ireland.

References

[1] C. Akerlof et al., Ap. J. 377 (1991) L97.
[2] D. Alexandreas et al., Proc. 23rd ICRC, Calgary, Vol. 1 (1993) p. 428.
[3] M. Amenomori et al., Proc. 24th ICRC, Rome, Vol. 2 (1995) p. 112.
[4] S. Barwick et al., Proc. 24th ICRC, Rome, Vol. 2 (1995) p. 436.
[5] M.F. Cawley et al., Exp. Astron. 1 (1991) 173.
[6] V. Connaughton et al., AIP Conf. Proc. 307 GRB, G.J. Fishman, J.J. Brainerd, K. Hurley, eds. (Huntsville, AL, 1993) p. 470.
[7] V. Connaughton et al., Ap. J. 479 (1997) 859.
[8] C. Fichtel et al., AIP Conf. Proc. 384 GRB, C. Kouveliotou, M.S. Briggs, G.J. Fishman, eds. (Huntsville, AL, 1995) p. 368.
[9] G.J. Fishman, C. Meegan, Annu. Rev. Astron. Astrophys. 33 (1995) 415.
[10] V.P. Fomin et al., Astropart. Phys. 2 (1994) 137.
[11] B. Funk et al., Proc. 24th ICRC, Rome, Vol. 2 (1995) p. 104.
[12] F. Halzen et al., Nature 353 (1991) 807.
[13] S.W. Hawking, Nature 248 (1974) 30.
[14] K. Hurley, Space Sc. Rev. 75 (1996) 43.
[15] M.P. Kertzmann, G.S. Sembroski, Nucl. Inst. Meth. A 343 (1994) 629.
[16] K. Nolan et al., Proc. 21 st. ICRC, Adelaide, Vol. 2 (1990) 150.
[17] N.A. Porter, T.C. Weekes, MNRAS 183 (1978) 285.
[18] N.A. Porter, T.C. Weekes, Nature 277 (1979) 199.
[19] M. Punch et al. Nature 358 (1992) 477.
[20] J. Quinn et al., Ap. J. 452 (1996) 588.
[21] P.T. Reynolds et al., Ap. J. 404 (1993) 206.
[22] T. Samura, K. Kobayakawa, Proc. 23rd ICRC, Calgary, Vol. 1 (1993) p. 128.
[23] P. Sommers, J.W. Elbert, J. Phys. G 13 (1987) 553.
[24] G. Vacanti et al., Ap. J. 377 (1991) 467.
[25] T.C. Weekes, Space Sci. Rev. 75 (1996) 1.